Micromotors with Step-Motor Characteristics by Controlled Magnetic Interactions among Assembled Components

Kwanoh Kim,[†] Jianhe Guo,[‡] Xiaobin Xu,[‡] and Donglei (Emma) Fan[*,†,‡]

[†]Department of Mechanical Engineering, the University of Texas at Austin, Austin, Texas 78712, United States, and [‡]Materials Science and Engineering Program, the University of Texas at Austin, Austin, Texas 78712, United States

ABSTRACT In this study, we investigated the control of the rotation dynamics of an innovative type of rotary micromotors with desired performances by tuning the magnetic interactions among the assembled micro/nanoscale components. The micromotors are made of metallic nanowires as rotors, patterned magnetic nanodisks as bearings and actuated by external electric fields. The magnetic forces for anchoring the rotors on the bearings play an essential role in the rotation dynamics of the micromotors. By varying the moment, orientation, and dimension of the magnetic components, distinct rotation behaviors can be observed, including repeatable wobbling and rolling in addition to rotation. We understood the rotation behaviors by analytical modeling, designed and realized micromotors with step-motor characteristics. The outcome of this research could inspire the development of high-performance nanomachines assembled from synthetic nanoentities, relevant to nanorobotics, microfluidics, and biomedical research.

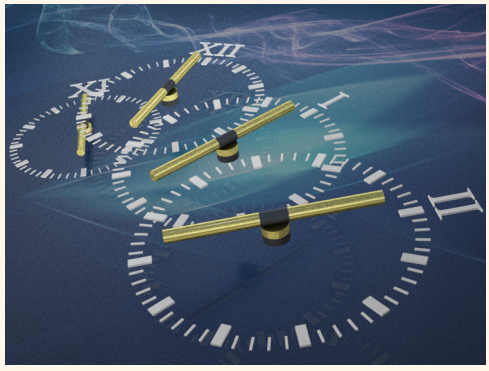

KEYWORDS: micromotors · nanomotors · step motors · assembly · electric tweezers · nanorobotics · nanoelectromechanical systems (NEMS)

Micro/Nanoelectromechanical systems (MEMS/NEMS) have attracted intense research interest for decades due to their promising applications across various research fields including electronics,[1,2] chemical and biomedical sensing,[3−6] and biochemical delivery.[7−11] Rotary nanomotors, a type of rotational NEMS devices, which can convert rotary motion into linear motion for powering and actuation, have attracted intense attention due to its critical role in advancing NEMS technology.[12−17]

Recently, an innovative type of rotary nanomotors has been bottom-up assembled from nanoscale building blocks by using the electric tweezers[18,19] and reported by our group.[20] The nanomotors were assembled into arrays and rotated with highly controlled angle, speed (to at least 18 000 rpm) and chirality. They could be rotated continuously for 15 h and applied in tunable biochemical release.[21] Although remarkably controllable and precise, the rotation speed of the nanomotors showed periodic fluctuation. We believe that the rotation speed fluctuation originated from the angle-dependent magnetic interactions between the rotors and bearing, which was used for the anchorage of the nanorotors. Therefore, it is highly desirable to eliminate the fluctuation of the interactions between the assembled components of the nanomotors for high performance in stability, controllability, and reliability.

In this work, we investigated the rotation dynamics of bottom-up assembled rotary motors by designing various configuration of magnetic interactions between the assembled subcomponents. Magnetic components with desired moment, orientation, and dimensions are successfully fabricated, which enabled distinct rotation behaviors from wobbling and self-rolling besides in-plane rotation to rotation at uniform speeds and stopping at designated angles, like step motors.

* Address correspondence to dfan@austin.utexas.edu.

Received for review October 10, 2014 and accepted December 23, 2014.

Published online December 23, 2014
10.1021/nn505798w

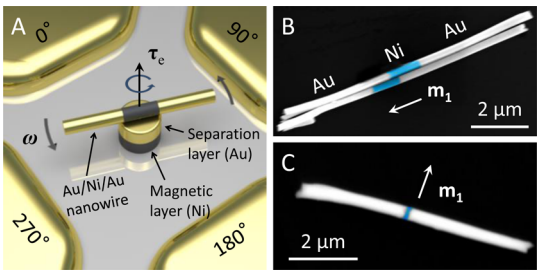

Figure 1. Structure of the nanomotor and the nanowire rotors. (A) Schematic diagram of a nanowire motor with a nanowire, magnetic bearing, and quadrupole electrodes as the rotor, bearing, and stator. (B and C) Scanning electron microscopy images of Au/Ni/Au nanowires with a (B) 1-μm- or (C) 100-nm-long Ni segment highlighted in blue. m_1 is the magnetic moment of the Ni segment of the nanowires.

RESULTS AND DISCUSSION

The motors consist of nanowires, patterned nanomagnets, and quadrupole microelectrodes serving as rotors, bearings, and stators, respectively (Figure 1A). An AC electric field (*E*-field) was applied to compel the motors to rotate *via* four AC electric voltages on a quadruple microelectrode with sequential 90° phase shifts.[16,20] To minimize the effect of Brownian motions on the rotation of motors and clearly understand the effect of magnetic interactions, we used nanowires with a length of ~10−7 μm and referred to the devices as micromotors in this work, although the devices can be made at a nanoscale with all components less than 1 μm (Supporting Information Video S1).[20]

Multisegment Au/Ni nanowires were fabricated by electrodeposition into nanoporous templates.[22] The magnetic strength and anisotropy of the nanowires were controlled by the geometry and total volume of the integrated magnetic segments in a blue false color in Figure 1B,C. For instance, the magnetic orientation of a nanowire with a 1-μm-long Ni segment is in the long direction of the nanowire (Figure 1B), while that of a nanowire with a 100-nm-long Ni segment is in the transverse direction (Figure 1C). More scanning electron microscopy (SEM) characterizations and analysis of size and composition distributions of nanowires are provided in the Supporting Information (Figure S1 and Table S1).

Magnetic bearings with diameters of 200 nm to 2 μm are patterned in the center of the quadrupole microelectrodes by colloidal nanolithography[23] or electron-beam lithography as shown in Supporting Information Figure S2 and Table S2. The magnetic bearings consist of a stack of thin films of N/M/Cr (6 nm), where N is a nonmagnetic spacer layer for controlling the magnetic forces between the rotors and bearings. They are typically made of pure Au (100 nm) or Au (100 nm) coated with a thin layer of carbon (3−4 nm). M is a magnetic layer made of either Ni with in-plane anisotropy (80 nm in thickness, deposition rate <0.5 Å/s in electron-beam evaporation) or CoPt alloys with perpendicular magnetic anisotropy (PMA, 20 nm in thickness). In all of our experiments, the bearings were first demagnetized with gradually decaying alternating magnetic fields and then remagnetized at 1 T for 50 s in the direction of magnetic anisotropy to achieve full saturation. Arrays of micromotors can be swiftly assembled by the electric tweezers.[8,19] The details are discussed in the Methods section.

To investigate how the rotation dynamics are tuned by the magnetic interactions between the assembled components, we studied three primary configurations: (1) chopstick configuration, both magnetic moments of the nanowire and the bearing are parallel to the plane of rotation; (2) perpendicular configuration, both magnetic moments of the nanowire and the bearing are perpendicular to the plane of rotation; and (3) T configuration, magnetic moment of the nanowire is parallel, while that of the bearing is perpendicular, to the plane of rotation.

For the chopstick configuration (Figure 2A), a micromotor made of a 4.5/1/4.5-μm-long Au/Ni/Au nanowire (Figure 1B) and a 1 μm diameter Ni bearing was assembled. Magnetic moment of the Ni segment (m_1) is along the long axis of the nanowire due to the shape anisotropy.[24] The Ni bearing exhibits a strong in-plane magnetic anisotropy (Figure 2B) also due to shape anisotropy. In this configuration, the rotation speed of micromotors oscillated as a function of the angular position with a period of 360° (Figure 2C and Supporting Information Video S2). Although the speed fluctuated periodically, the overall rotation was stable, since the center of the nanowire (Figure 2D) and the instant center of rotation (Figure 2E) barely moved apart from the center of the bearing. From this, it can be readily known that the nanowire rotated with both ends of the 1-μm-long Ni segment flushing with the edge of the 1 μm diameter bearing, which resulted in balanced and symmetric rotation without significant lateral motion or wobbling (Figure 2F).

The periodic oscillation of rotation speed (ω) can be understood by the torque involved in the micromotors given by[20]

$$\tau_e + \tau_{e'} + \tau_\eta + \tau_m + \tau_f = 0 \qquad (1)$$

where τ_η, τ_m, and τ_f are viscous drag, magnetic, and friction torques, respectively. τ_e and $\tau_{e'}$ are torques due to interaction between the polarized nanowire and the external *E*-field (*E*) and that between the polarized nanowires and bearings, respectively. The detailed modeling has been reported elsewhere and discussed here in brief: both τ_e and $\tau_{e'}$ are proportional to E^2 and $\tau_\eta \sim \omega$;[25,26] therefore, $\tau_e = aE^2$, $\tau_{e'} = bE^2$, and $\tau_\eta = c\omega$, where *a*, *b*, and *c* are constants. The magnetic torque (τ_m) is due to the magnetic interaction between the Ni segment in the nanowire rotor and the patterned magnetic bearing, which depends on the angle

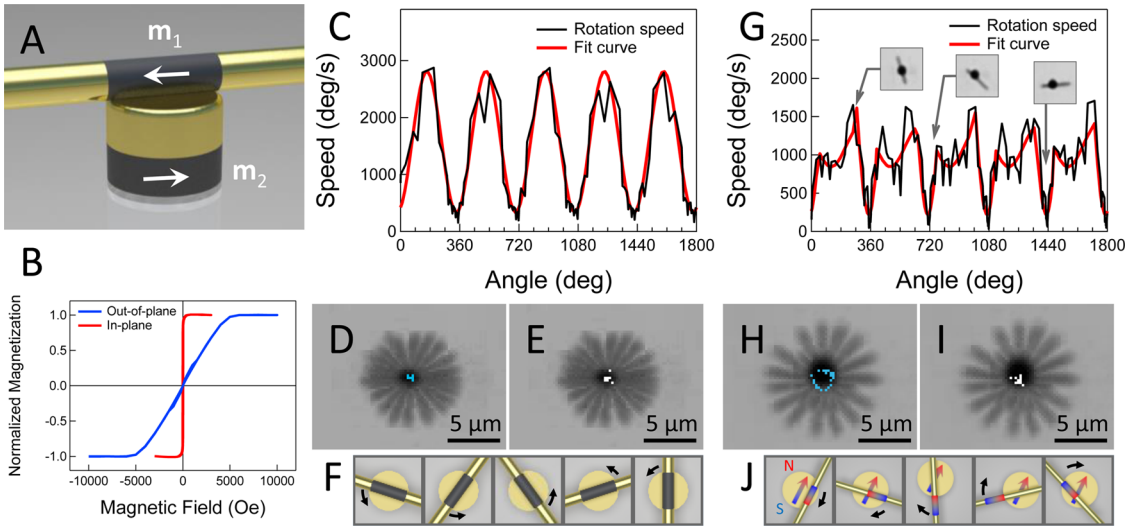

Figure 2. Characteristics of micromotors with the chopstick configuration. (A) Schematic diagram of a motor with the magnetic moment of the nanowire and the bearing parallel to the substrate. (B) Vibrating sample magnetometer (VSM) measurement showing the in-plane magnetic anisotropy of a Ni thin film. (C−F) Rotation of a micromotor with a 1:1 ratio of the length of the Ni segment and diameter of the bearing: (C) rotation speed as a function of the angular position of the nanowire; (D) center of the nanowire rotor; (E) instant center of rotation; and (F) diagram of a nanowire rotating on the bearing. (G−J) Rotation of a micromotor with a 1:2 ratio of the length of the Ni segment and diameter of the bearing: (G) rotation speed as a function of the angular position of the nanowire; (H) center of the nanowire rotor; (I) instant center of rotation; and (J) diagram of a nanowire rotating on the bearing.

(Θ) between the magnetic moment of the nanowire m_1 (θ) and magnetic bearing m_2 (θ_m), given by $\Theta = \theta - \theta_m$. If we simplify the magnetic rotor and bearing as two magnetic dipoles separated at a distance r, the magnetic force (F_m) and torque (τ_m) exerted on the nanowire can be given by $F_m = 3\mu_0(m_1 m_2 \cos\Theta)/(4\pi r^4)$ and $\tau_m = \mu_0(m_1 m_2 \sin\Theta)/(4\pi r^3)$, respectively, where μ_0 is the magnetic permittivity of vacuum magnetic force. Therefore, it can be known that $\tau_m = d \sin\Theta$ and $\tau_f = e\cos\Theta + f$, where d, e, and f are constants. As a result, eq 1 can be rewritten as

$$\omega(\theta) = \frac{d}{-c}\sin(\theta - \theta_m) + \frac{e}{-c}\cos(\theta - \theta_m) + \frac{(a+b)E^2 + f}{-c} \quad (2)$$

It is clear that the torques due to the magnetic interaction, such as τ_m and τ_f, induced the oscillation of the rotation speed. The observed angular dependence of rotation speed can be well fitted by eq 2 (red curve in Figure 2C), which suggests the validity of our modeling.

Even at the simple chopstick configuration, it is interesting to know how the relative strength and dimensions of the assembled magnetic components can be used to tune the rotation dynamics of micromotors. In addition to the first case with the 1:1 dimension ratio, the magnetic components of the nanomotor were designed to have a 1:2 ratio, *i.e.*, a 1-μm-long Ni segment in the rotor and 2 μm diameter for the bearing. The same rotation periodicity of 360° was observed as that of the motors discussed above (dimension ratio 1:1), but a local minimum at ~180° with two asymmetric peaks emerged evidently (Figure 2G). It is also noticed that the center of the nanowire moved around forming a circle of ~2 μm in diameter (Figure 2H), while the trajectory of the instant center of rotation was closely packed in a small area, both located at the lower half of the bearing (Figure 2I). After careful frame-by-frame image analysis, we found that the nanowire rotated with the edge of the Ni segment flushing with that of the magnetic bearing, but alternately staying atop and hanging over the side of the bearing (Figure 2J). This rotation behavior is a result of the minimization of the magnetic repulsive energy by having antiparallel magnetic configurations in a side-by-side or stacked configuration as shown in Figure 2J (south and north poles (i) overlap; (ii) next to each other). Since the magnetic forces for these two antiparallel configurations are in opposite directions and distinct in strength, a rotation periodicity of ~180° and two asymmetric peaks can be observed. With the above understanding, we fitted the rotation speed using two sine waves with different amplitudes and phases (red curve in Figure 2G). A much better fitting curve that matches the experiments can be obtained compared to that with a single sine wave.

Next, we further reduced the aspect ratio of the Ni segments of the nanowires to form thin Ni disks (300 nm in diameter and 100 nm in thickness) and rotated them on 1 μm Ni bearings. Now the magnetic moments of the rotors are transverse to their long direction (Figure 1C). Different from the two aforediscussed parallel-configured micromotors in Figure 2, a strong rotation periodicity of 180° was found (Figure 3A). Here none of the model introduced above can be used to fully understand the rotation behaviors of this configuration. Moreover, although the nanowire rotors

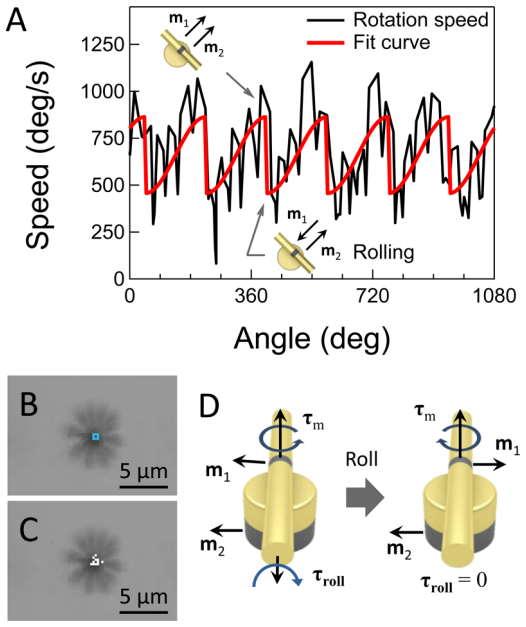

Figure 3. Rotation dynamics of a micromotor with a thin Ni segment of 100 nm in thickness anchoring on a Ni bearing of 1 μm in diameter. (A) Rotation speed as a function of angle. (B) Center of the nanowire rotor and (C) the instant center of rotation. (D) Schematic diagrams showing the rolling of the nanowire rotor along the long axis, which results in antiparallel alignment of the magnetic moments of the rotor and bearing.

wobbled on the bearings (Figure 3B,C), it is difficult to conclude that the magnetic segment of the rotors hung over the side of the magnetic bearings as that in Figure 2J. With careful analysis, we suggest that the 180° periodic oscillation originates from the self-rolling of the nanowires along the long direction of the nanowire during its in-plane rotation, which effectively changed the unstable repulsive magnetic configuration to a stable attractive magnetic configuration every 180° as shown in the schematic diagram of Figure 3D. It is also found that the rotation speed dropped abruptly, while increased gradually (Figure 3A), which could be an evidence of the abrupt change in magnetic configuration induced by the self-rolling. Besides, the rotation speed fits well to the half of a sine wave from the negative peak to the positive peak, *i.e.*, $\omega = A \sin(\theta - \phi)$ at $-\pi/2 + \phi \leq \theta < \pi/2 + \phi$, repeating every 180° (red curve in Figure 3A). It can also support the self-rolling mechanism by which the magnetic orientation of the Ni segment of the nanowire is flipped and set to 0 relative to that of the bearing every 180°. As a result, this kind of motors has two syngenetic periodic rotations, one is along the direction of nanowires and the other is in the horizontal plane.

Note that the fit-curves in Figure 2G and Figure 3A have certain deviation from the experimental curves. It can be attributed to the more complex rotation dynamics of the nanomotors, whose motion trajectories could slightly change in each cycle and result in noises and deviations among different cycles. It can be also because the fitted curves are based on a simple magnetic dipole−dipole model, without consideration of the position dependent magnetic force at different locations on the bearings when the rotors are rotating atop of the bearings for both cases in Figure 2G and 3A. Also, we used an effective distance between the magnetic dipoles in the model for Figure 2G when the magnetic segment of the rotor was hanging over the side of the bearing, without further considering the complex temporal distance change. Nevertheless, the fit-curves match the data for both cases in large, which supports the feasibility of our analysis and understanding of the behavior of the motors.

The most interesting magnetic configuration we examined is the perpendicular configuration, where both the magnetic moments of the nanowires and bearings are perpendicular to the plane of rotation (Figure 4A). To construct such micromotors, we used nanowires with transverse magnetic anisotropy (Figure 1C) and bearings made of PMA alloys with strong perpendicular magnetic anisotropy as shown in the polar Kerr measurement (Figure 4B, 1 μm to 200 nm in diameter). Since m_1 and m_2 are parallel to each other and both of them are perpendicular to the rotation plane, the magnetic force, given by $F_m = 3\ \mu_0\ (m_1 m_2)/(2\pi r^4)$, as well as the resulting frictional torque remain constant regardless of the angular position of the nanowire. Also the angle-dependent magnetic torque vanishes from eq 1, which is distinctly different from that of the parallel configuration. As a result, the motors can rotate with uniform speed without observable periodic oscillation (Figure 4C and Supporting Information Video S2), even at high voltages (Figure 4D). They can be compelled to rotate and stop at designated angles, very much like step motors, by simply controlling the intensity and pulse duration of the applied *E*-field (Figure 4E, Supporting Information Video S3, and Table S3). This type of micromotors could be more advantageous for applications in practice due to the uniform rotation speeds, controlled angular positions, and high stability, compared to those with chopstick configurations. Note that the chopstick-configured micromotors always restore to align with the magnetic moment of the bearing after removal of the *E*-field, regardless of the final angular position set by the *E*-field, even for those motors whose dimensions are all smaller than 1 μm (Supporting Information Video S1 and S4).

We also note that the angular step of the nanowire rotors has a relative standard deviation (%RSD) of 3.7% − 20.0%. The overall %RSD decreases with the increase of the designed angular step size in general (Table S3 in Supporting Information). The standard deviation of the rotation angle remains largely the same when the preset angle is less than 190° and approximately doubled when the rotation angle is 260° and above. This variation in the angular displacement can be

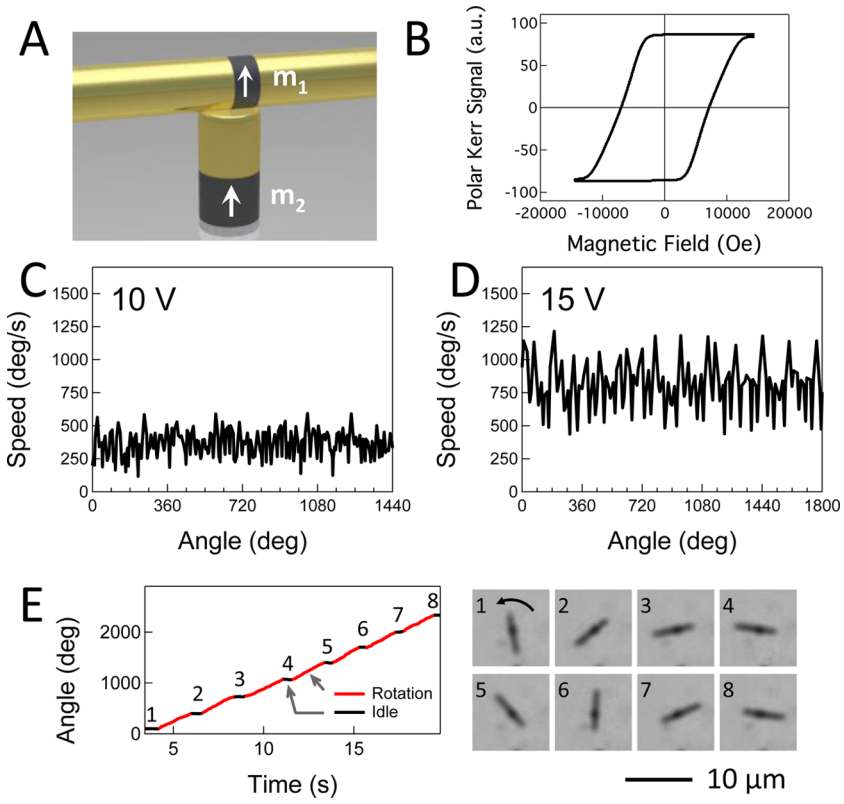

Figure 4. Characterization of a nanowire with the perpendicular magnetic configuration (100-nm-long Ni segment in the rotor and PMA bearing with 1 μm in diameter). (A) Schematic diagram of the magnetic configuration of the micromotor. (B) Polar Kerr measurement in the vertical direction showing the perpendicular magnetic anisotropy of the PMA alloy thin film. (C and D) Rotation speed as a function of angle at various voltages, *e.g.*, (C) 10 V and (D) 15 V. (E) Rotation of a micromotor with controlled angular displacement *versus* time, resembling step motors, and snap shots of the micromotor at the designated angular displacement.

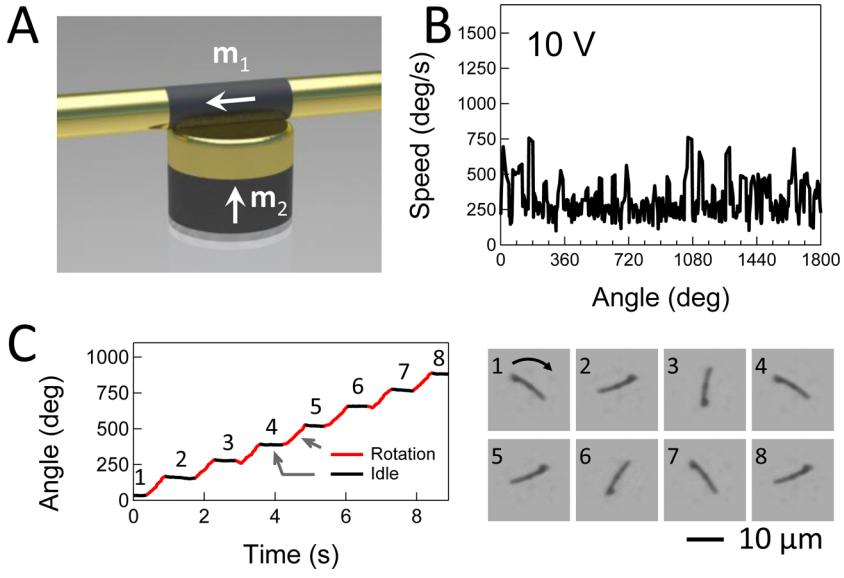

Figure 5. Characteristics of a micromotor with a "T" shaped magnetic configuration with a 1-μm-long Ni segment in the rotor assembled on a PMA bearing of 1 μm in diameter. (A) Schematic diagram of the motor. (B) Rotation speed as a function of angular position. (C) Angular position of a micromotor with controlled angular displacement as a function of time and the enhanced snapshots of the micromotor at the idle position indicated in the angle-time plot.

attributed to the imperfect synchronization of the four AC voltages applied to the electrodes. For the rotation with larger angular displacement, the nonuniform interface between a bearing and a rotor and the Brownian motion can also affect the rotation significantly, which makes the angular displacement more

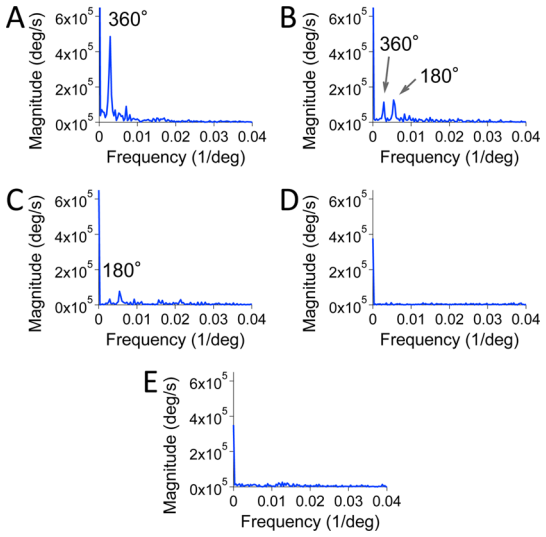

Figure 6. Fourier transforms of rotation speed *versus* time of micromotors with different magnetic configurations. (A) Chopstick configuration with a 1-μm-long Ni segment in the rotor on a Ni bearing of 1 μm in diameter. (B) Chopstick configuration with a 1-μm-long Ni segment in the rotor on a Ni bearing of 2 μm in diameter. (C) Chopstick configuration with a 100-nm-long Ni segment in the rotor on a Ni bearing of 1 μm in diameter. (D) Perpendicular configuration with a 100-nm-long Ni segment in the rotor on a PMA bearing of 1 μm in diameter. (E) T-shaped configuration with a 1-μm-long Ni segment in the rotor on a PMA bearing of 1 μm in diameter.

deviate. Therefore, the angular control precision of the motors is expected to be well improved by refining the *E*-field control program and circuit, enhancing the surface smoothness of the bearings, and implementing mechanisms to counter the Brownian motions of the nanorotors.[27]

The last type of motor has a "T" shaped magnetic configuration (Figure 5A). The nanomotor is built from a nanowire rotor with a 1-μm-long Ni segment whose magnetic moment is parallel to the plane of rotation, and a PMA bearing with its magnetic moment perpendicular to the plane of rotation. The magnetic configuration is in a "T" shape. Under this condition, the magnetic torque and force can be calculated to be $F_m \sim \mu_0 m_1 m_2/\pi r^4$ and $\tau_m \sim \mu_0 m_1 m_2/\pi r^3$, respectively, both of which are independent of the angular position of the nanowire. As a result, this type of micromotor shows a similar rotation behavior with that of aforediscussed perpendicularly configured micromotors. The rotation speed is highly uniform (Figure 5B and Supporting Information Video S2) and the angular position of the rotor can be controlled with arbitrary angular steps (Figure 5C and Supporting Information Video S5).

Finally, the characteristic rotation speed spectra of all the different types of micromotors were processed with Fourier transformation. It can be found that all the parallel configured micromotors showed strong periodicity of 360° and/or 180°, agreeing with our conclusions (Figure 6A–C and Supporting Information Video S2). In comparison, the typical Fourier transformation of the perpendicular- and T-configured micromotors is nearly a flat line, without any clear periodicity (Figure 6D,E, and Supporting Information Video S2). This corroborates the successful achievement of the micromotors with uniform rotating speeds by manipulating magnetic interactions between assembled components.

CONCLUSION

In summary, we investigated rotation dynamics of bottom-up assembled rotary micromotors by tuning the magnetic interactions among different assembled nanoentities. Various magnetic configurations were designed and successfully implemented with controlled strength, orientation, and dimensions, which resulted in distinct rotation behaviors including repeatable wobbling and self-rolling in addition to in-plane rotation. We understood the rotation behaviors by modeling the magnetic interactions. With these understanding, high-performance micromotors have been rationally designed and successfully achieved, where the micromotors rotate at uniform speeds and position at desired angles, resembling step motors. Our findings could assist the development of nanomotors with desirable performances for various applications and impact research areas including NEMS, microfluidics, and nanobiotechnology.

METHODS

The micromotors were assembled by the electric tweezers.[18,19] In brief, by using the combined AC and DC *E*-fields, nanowires suspended in deionized (DI) water were manipulated in both the *X* and *Y* directions to the magnetic bearings. When in the vicinity of the magnetic bearings, they can be swiftly attracted and assembled atop of the bearings.[20,28] Here, the magnetic force between the magnetic elements in the rotors and bearings is controlled by the Au separation layers (Figure 1A), thereto anchors the rotors on the bearings while still allowing the rotation. The rotation of the micromotors was captured by a digital camera equipped on an optical microscope operating at 50–60 frames per second (fps).

Conflict of Interest: The authors declare no competing financial interest.

Acknowledgment. This research was supported by National Science Foundation (NSF) CAREER Award (Grant No. CMMI 1150767), Welch Foundation (Grant No. F-1734), NIH (9R42ES024023-02) and NSF grant (ECCS-1446489) in part, and Research Grant from the Vice President Office for Research at UT-Austin. The authors thank Frank Q. Zhu for help with deposition of PMA thin films and the magnetic characterization.

Supporting Information Available: Videos of continuous and discrete rotation of nano/micromotors with different magnetic configurations, tables showing the size and composition distribution of nanowires and patterned magnetic bearings, and statistical analysis of rotation of micromotors with step-motor characteristics are supplied. This material is available free of charge *via* the Internet at http://pubs.acs.org.

REFERENCES AND NOTES

1. Lee, J. O.; Song, Y.-H.; Kim, M.-W.; Kang, M.-H.; Oh, J.-S.; Yang, H.-H.; Yoon, J.-B. A Sub-1-V Nanoelectromechanical Switching Device. *Nat. Nanotechnol.* **2012**, *8*, 36–40.
2. Feng, X. L.; Matheny, M. H.; Zorman, C. A.; Mehregany, M.; Roukes, M. L. Low Voltage Nanoelectromechanical Switches Based on Silicon Carbide Nanowires. *Nano Lett.* **2010**, *10*, 2891–2896.
3. Li, M.; Tang, H. X.; Roukes, M. L. Ultra-Sensitive NEMS-Based Cantilevers for Sensing, Scanned Probe and Very High-Frequency Applications. *Nat. Nanotechnol.* **2007**, *2*, 114–120.
4. Hanay, M. S.; Kelber, S.; Naik, A. K.; Chi, D.; Hentz, S.; Bullard, E. C.; Colinet, E.; Duraffourg, L.; Roukes, M. L. Single-Protein Nanomechanical Mass Spectrometry in Real Time. *Nat. Nanotechnol.* **2012**, *7*, 602–608.
5. Xu, X.; Li, H.; Hasan, D.; Ruoff, R. S.; Wang, A. X.; Fan, D. L. Near-Field Enhanced Plasmonic-Magnetic Bifunctional Nanotubes for Single Cell Bioanalysis. *Adv. Funct. Mater.* **2013**, *23*, 4332–4338.
6. Campuzano, S.; Kagan, D.; Orozco, J.; Wang, J. Motion-Driven Sensing and Biosensing Using Electrochemically Propelled Nanomotors. *Analyst* **2011**, *136*, 4621–4630.
7. Guix, M.; Mayorga-Martinez, C. C.; Merkoçi, A. Nano/Micromotors in (Bio)chemical Science Applications. *Chem. Rev.* **2014**, *114*, 6285–6322.
8. Fan, D.; Yin, Z.; Cheong, R.; Zhu, F. Q.; Cammarata, R. C.; Chien, C. L.; Levchenko, A. Subcellular-Resolution Delivery of a Cytokine through Precisely Manipulated Nanowires. *Nat. Nanotechnol.* **2010**, *5*, 545–551.
9. Douglas, S. M.; Bachelet, I.; Church, G. M. A Logic-Gated Nanorobot for Targeted Transport of Molecular Payloads. *Science* **2012**, *335*, 831–834.
10. Wang, J. Cargo-Towing Synthetic Nanomachines: Towards Active Transport in Microchip Devices. *Lab. Chip* **2012**, *12*, 1944–1950.
11. Wang, W.; Duan, W.; Ahmed, S.; Mallouk, T. E.; Sen, A. Small Power: Autonomous Nano- and Micromotors Propelled by Self-Generated Gradients. *Nano Today* **2013**, *8*, 531–554.
12. Fennimore, A. M.; Yuzvinsky, T. D.; Han, W.-Q.; Fuhrer, M. S.; Cumings, J.; Zettl, A. Rotational Actuators Based on Carbon Nanotubes. *Nature* **2003**, *424*, 408–410.
13. Fournier-Bidoz, S.; Arsenault, A. C.; Manners, I.; Ozin, G. A. Synthetic Self-Propelled Nanorotors. *Chem. Commun.* **2005**, 441–443.
14. Yuzvinsky, T. D.; Fennimore, A. M.; Kis, A.; Zettl, A. Controlled Placement of Highly Aligned Carbon Nanotubes for the Manufacture of Arrays of Nanoscale Torsional Actuators. *Nanotechnology* **2006**, *17*, 434–438.
15. Soong, R. K.; Bachand, G. D.; Neves, H. P.; Olkhovets, A. G.; Craighead, H. G.; Montemagno, C. D. Powering an Inorganic Nanodevice with a Biomolecular Motor. *Science* **2000**, *290*, 1555–1558.
16. Fan, D.; Zhu, F.; Cammarata, R.; Chien, C. Controllable High-Speed Rotation of Nanowires. *Phys. Rev. Lett.* **2005**, *94*.
17. Xu, X.; Liu, C.; Kim, K.; Fan, D. L. Electric-Driven Rotation of Silicon Nanowires and Silicon Nanowire Motors. *Adv. Funct. Mater.* **2014**, *24*, 4843–4850.
18. Fan, D. L.; Cammarata, R. C.; Chien, C. L. Precision Transport and Assembling of Nanowires in Suspension by Electric Fields. *Appl. Phys. Lett.* **2008**, *92*, 093115.
19. Fan, D. L.; Zhu, F. Q.; Cammarata, R. C.; Chien, C. L. Electric Tweezers. *Nano Today* **2011**, *6*, 339–354.
20. Kim, K.; Xu, X.; Guo, J.; Fan, D. L. Ultrahigh-Speed Rotating Nanoelectromechanical System Devices Assembled from Nanoscale Building Blocks. *Nat. Commun.* **2014**, *5*, 3632.
21. Xu, X.; Kim, K.; Fan, D. Tunable Release of Multiplex Biochemicals by Plasmonically Active Rotary Nanomotors. *Angew. Chem., Int. Ed.* DOI: 10.1002/anie.201410754, (http://onlinelibrary.wiley.com/journal/10.1002/(ISSN)1521-3773/homepage/2002_preview.html).
22. Whitney, T. M.; Searson, P. C.; Jiang, J. S.; Chien, C. L. Fabrication and Magnetic Properties of Arrays of Metallic Nanowires. *Science* **1993**, *261*, 1316–1319.
23. Fan, D. L.; Kim, K.; Guo, J. Electrode Design and Low-Cost Fabrication Method for Assembling and Actuation of Nanomotors with Ultrahigh and Uniform Speed. Provisional International Patent Application 62047969, 2014.
24. Sun, L.; Hao, Y.; Chien, C.-L.; Searson, P. C. Tuning the Properties of Magnetic Nanowires. *IBM J. Res. Dev.* **2005**, *49*, 79–102.
25. Keshoju, K.; Xing, H.; Sun, L. Magnetic Field Driven Nanowire Rotation in Suspension. *Appl. Phys. Lett.* **2007**, *91*, 123114.
26. Jones, T. B. *Electromechanics of Particles*; Cambridge University Press: Cambridge; New York, 2005.
27. Cohen, A. E.; Moerner, W. E. Suppressing Brownian Motion of Individual Biomolecules in Solution. *Proc. Natl. Acad. Sci. U.S.A.* **2006**, *103*, 4362–4365.
28. Kim, K.; Zhu, F. Q.; Fan, D. Innovative Mechanisms for Precision Assembly and Actuation of Arrays of Nanowire Oscillators. *ACS Nano* **2013**, *7*, 3476–3483.